The 2013 World Congress on
Advances in Structural Engineering and Mechanics (ASEM13)
Jeju, Korea, September 8-12, 2013

Finite cylindrical prism methods for the analysis of laminated composite hollow cylinders

*Chih-Ping Wu[1)] and Hao-Yuan Li[2)]

[1), 2)] *Department of Civil Engineering, National Cheng Kung University, Tainan 70101, Taiwan, ROC*
[1)]cpwu@mail.ncku.edu.tw

ABSTRACT

A unified formulation of finite cylindrical prism methods (FCPMs), based on the Reissner mixed variational theorem (RMVT), is developed for the three-dimensional (3D) analysis of laminated circular hollow cylinders with various boundary conditions and under mechanical loads. In this formulation, the cylinder is divided into a number of finite cylindrical prisms, in which the trigonometric functions and Lagrange polynomials are used to interpolate the circumferential direction and the axial-radial surface variations of the primary field variables of each individual prism, respectively. The number of nodes of the nodal surface of each prism can be set at four for linear FCPMs, and eight and nine for quadratic ones. The present quadratic FCPM solutions of simply supported, laminated composite cylinders are in excellent agreement with the exact 3D solutions available in the literature, and these for the cylinders with combinations of clamped and simply-supported edge conditions closely agree with the solutions obtained using the ANSYS commercial software.

1. INTRODUCTION

In recent decades, laminated composite (LC) structures have attracted considerable attention in advanced engineering applications due to their high strength- and stiffness-to-weight ratios. In order to achieve a reliable design to enhance the working lifetime of LC structures, various three-dimensional (3D) numerical modeling and theoretical methodologies have been proposed in the open literature to assess the performances of assorted two-dimensional (2D) ones. The review articles with regard to a variety of 3D and 2D computational models of LC structures have been carried out by Noor and Burton (1990a, b), Noor et al. (1991, 1996), Carrera (2000a, b,c, 2001, 2003), Carrera et al. (2010), Carrera and Ciuffreda (2005), Carrera and Petrolo (2010), and Wu et al. (2008). Note that among these literature, most of the 3D solutions were obtained for the plates/shells with fully simple supports, and few for other boundary conditions, such as fully clamped edges, and combinations of clamped, and simply-supported ones.

Based on the principle of virtual displacement (PVD), Cheung and Jiang (2001) developed a finite layer method (FLM) for the 3D static analysis of simply-supported, piezoelectric composite laminates, and it was also extended to the 3D static, vibration,

stability and thermal buckling analyses of simply-supported, piezoelectric composite plates by Akhras and Li (2007, 2008, 2010), in which this PVD-based FLM was demonstrated to be more effective in reducing computational effort and core requirements for simply-supported laminates. Subsequently, based on the RMVT instead of the PVD, Wu and Li (2010), and Wu and Chang (2012) developed the unified formulations of the finite rectangular layer methods (FRLMs) and the finite cylindrical layer methods (FCLMs) for the 3D analysis of simply-supported, LC plates/cylinders, in which the relative orders used for expansion of the displacement and transverse stress components through the thickness coordinate can be freely chosen.

After a close review of the literature, as summarized above, we found that relatively few published articles deal with the mechanical problems of LC structures with various boundary conditions using RMVT-based theories in comparison with those using the PVD-based ones, and most of the above-mentioned FRLMs and FCLMs are applicable to the 3D problems of LC plates/shells with fully simple supports, rather than other kinds of edges, such as clamped ones. The current study therefore aims at developing a unified formulation of the RMVT-based finite cylindrical prism methods (FCPMs) for the approximate 3D analysis of LC cylinders with combinations of clamped and simply-supported conditions at the edges. In the following illustrative examples, these RMVT-based FCPMs with the relevant orders are taken to be linear or quadratic, which are four-node linear (L4), and eight- and nine-node quadratic (Q8 and Q9) FCPMs. The accuracy and convergence of these FCPMs are examined by comparing these FCPM solutions with both the 3D elasticity solutions of simply-supported, LC cylinders and the accurate solutions obtained using the ANSYS commercial software for LC cylinders with various boundary conditions. In addition, a parametric study with regard to various effects on the displacement and stress components that are induced in LC cylinders is carried out, such as the radius-to-thickness and length-to-radius ratios, and different boundary conditions.

2. RMVT-BASED FINITE CYLINDRICAL PRISM METHODS

2.1. Kinematic and kinetic assumptions

We consider an LC cylinder subjected to a sinusoidally (or uniformly) distributed load on either the inner or outer surface, as shown in Fig. 1*a*, in which the length and mid-surface radius of the cylinder are defined as *L* and *R*, respectively, and the edge conditions of this cylinder are considered as combinations of clamped, and simply-supported edges. The radial coordinate (*r*) is replaced by the thickness (ζ) one with the relation, $r = R + \zeta$, as used in this formulation. The cylindrical global and local coordinate systems (i.e., *x*, θ and ζ coordinates, and $\bar{x}$, $\bar{\theta}$ and $\bar{\zeta}$ coordinates) are located on the middle surface of the cylinder and a typical cylindrical prism, respectively, as shown in Figs. 1a and 1b, in which $x = x_e + \bar{x}$, $\theta = \bar{\theta}$ and $\zeta = \zeta_e + \bar{\zeta}$, and $(x_e,\ \zeta_e)$ denote the coordinates of the center of the typical cylindrical prism in the axial and thickness coordinates. The thicknesses of each individual prism and the cylinder are $h_m\ (m = 1, 2, \cdots, N_l)$ and *h*, respectively, while $h = \sum_{m=1}^{N_l} h_m$, in which N_l is the total number of the layers constituting the cylinder.

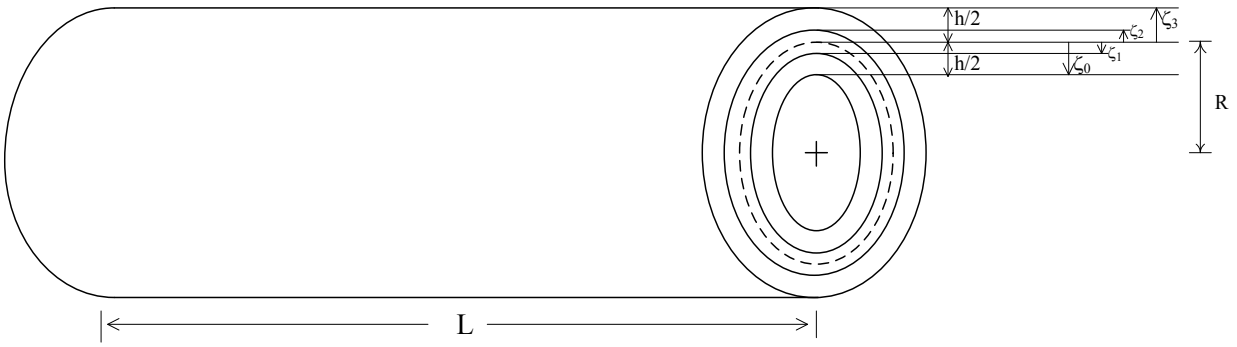

Fig. 1(a) The configuration and coordinates of a laminated composite cylinder

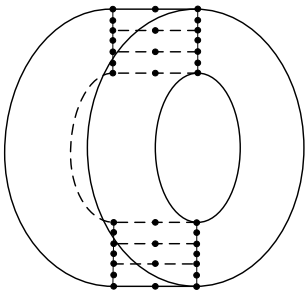

Fig. 1(b) The configuration of a three-layered cylindrical prism

The displacement components of a typical cylindrical prism of the m^{th}-layer are given by

$$\left[u_x^{(e)}(x,\,\theta,\,\zeta)\right]^{(m)} = \sum_{i=1}^{n_u} \left[\psi_u^{(e)}(x,\,\zeta)\right]_i \left[u^{(e)}(\theta)\right]_i^{(m)}, \tag{1}$$

$$\left[u_\theta^{(e)}(x,\,\theta,\,\zeta)\right]^{(m)} = \sum_{i=1}^{n_u} \left[\psi_u^{(e)}(x,\,\zeta)\right]_i \left[v^{(e)}(\theta)\right]_i^{(m)}, \tag{2}$$

$$\left[u_\zeta^{(e)}(x,\,\theta,\,\zeta)\right]^{(m)} = \sum_{j=1}^{n_w} \left[\psi_w^{(e)}(x,\,\zeta)\right]_j \left[w^{(e)}(\theta)\right]_j^{(m)}, \tag{3}$$

where $\left(u^{(e)}\right)_i^{(m)}$, $\left(v^{(e)}\right)_i^{(m)}$, $\left(w^{(e)}\right)_j^{(m)}$ with $(i=1,\,2,\,\cdots,\,n_u)$ and $\left(j=1,\,2,\cdots,n_w\right)$ are the nodal displacement components of a typical cylindrical prism of the m^{th}-layer of the cylinder; n_i=4, 8 and 9, in which *i*=*u* and *w*, denote the number of nodes of the L4, Q8 and Q9 prisms, respectively, the domains of which are $\left(x_e - a/2\right) \le x \le \left(x_e + a/2\right)$, $0 \le \theta \le 2\pi$ and $\left(\zeta_e - b/2\right) \le \zeta \le \left(\zeta_e + b/2\right)$, in which *a* and *b* are the dimensions of the rectangular section of the cylindrical prism, and their node numberings are shown in Fig. 2; while $\left(\psi_u^{(e)}\right)_i^{(m)}$ $(i=1,\cdots,n_u)$ and $\left(\psi_w^{(e)}\right)_j^{(m)}$ $(j=1,\,2,\cdots,n_w)$ are the corresponding shape functions.

The transverse shear and normal stress components are regarded as the primary variables in the RMVT-based FCPMs, and for a typical cylindrical prism of the m^{th}-layer these are assumed to be as follows:

$$\left[\tau_{x\zeta}^{(e)}(x,\,\theta,\,\zeta)\right]^{(m)}=\sum_{i=1}^{n_\tau}\left[\psi_\tau^{(e)}(x,\,\zeta)\right]_i\left[\tau_{13}^{(e)}(\theta)\right]_i^{(m)}, \tag{4}$$

$$\left[\tau_{\theta\zeta}^{(e)}(x,\,\theta,\,\zeta)\right]^{(m)}=\sum_{i=1}^{n_\tau}\left[\psi_\tau^{(e)}(x,\,\zeta)\right]_i\left[\tau_{23}^{(e)}(\theta)\right]_i^{(m)}, \tag{5}$$

$$\left[\sigma_{\zeta}^{(e)}(x,\,\theta,\,\zeta)\right]^{(m)}=\sum_{j=1}^{n_\sigma}\left[\psi_\sigma^{(e)}(x,\,\zeta)\right]_j\left[\sigma_{3}^{(e)}(\theta)\right]_j^{(m)}, \tag{6}$$

where $\left(\tau_{13}^{(e)}\right)_i^{(m)}$, $\left(\tau_{23}^{(e)}\right)_i^{(m)}$, $\left(\sigma_3^{(e)}\right)_j^{(m)}$ with $(i=1,\,2,\cdots,\,n_\tau)$ and $(j=1,2,\cdots,\,n_\sigma)$ are the nodal transverse stress components of a typical cylindrical prism of the m^{th}-layer of the cylinder; while $\left(\psi_\tau^{(e)}\right)_i$ $(i=1,\,2,\cdots,\,n_\tau)$ and $\left(\psi_\sigma^{(e)}\right)_j$ $(j=1,\,2,\cdots,n_\sigma)$ are the corresponding shape functions, in which n_τ and n_σ denote the number of nodes of the L4, Q8 and Q9 prisms, which are four, eight and nine, respectively.

The linear constitutive equations of the m^{th}-layer, which are valid for the orthotropic materials, are given by

$$\begin{Bmatrix}\sigma_x^{(m)}\\ \sigma_\theta^{(m)}\\ \sigma_\zeta^{(m)}\\ \tau_{\theta\zeta}^{(m)}\\ \tau_{x\zeta}^{(m)}\\ \tau_{x\theta}^{(m)}\end{Bmatrix}=\begin{bmatrix}c_{11}^{(m)} & c_{12}^{(m)} & c_{13}^{(m)} & 0 & 0 & 0\\ c_{12}^{(m)} & c_{22}^{(m)} & c_{23}^{(m)} & 0 & 0 & 0\\ c_{13}^{(m)} & c_{23}^{(m)} & c_{33}^{(m)} & 0 & 0 & 0\\ 0 & 0 & 0 & c_{44}^{(m)} & 0 & 0\\ 0 & 0 & 0 & 0 & c_{55}^{(m)} & 0\\ 0 & 0 & 0 & 0 & 0 & c_{66}^{(m)}\end{bmatrix}\begin{Bmatrix}\varepsilon_x^{(m)}\\ \varepsilon_\theta^{(m)}\\ \varepsilon_\zeta^{(m)}\\ \gamma_{\theta\zeta}^{(m)}\\ \gamma_{x\zeta}^{(m)}\\ \gamma_{x\theta}^{(m)}\end{Bmatrix}, \tag{7}$$

where $(\sigma_x^{(m)},\,\sigma_\theta^{(m)},\cdots,\tau_{x\theta}^{(m)})$ are the stress components; $(\varepsilon_x^{(m)},\,\varepsilon_\theta^{(m)},\cdots,\gamma_{x\theta}^{(m)})$ are the strain components; $c_{ij}^{(m)}$ are the elastic coefficients, which are constants through the thickness coordinate in the homogeneous elastic layers, and variable through the thickness coordinate in the FGM layers (i.e., $c_{ij}^{(m)}(\zeta)$).

2.2. The Reissner mixed variational theorem

The Reissner mixed variational theorem is used to derive the equilibrium equations of the cylinder, and its corresponding energy functional is written in the form of

$$\Pi_R = \int_{-h/2}^{h/2} \iint_{\Omega} \left[\sigma_x\, \varepsilon_x + \sigma_\theta\, \varepsilon_\theta + \sigma_\zeta\, \varepsilon_\zeta + \tau_{x\zeta}\gamma_{x\zeta} + \tau_{\theta\zeta}\gamma_{\theta\zeta} + \tau_{x\theta}\,\gamma_{x\theta} - B\left(\sigma_{ij}\right)\right](R+\zeta)\,dx\,d\theta\,d\zeta$$
$$- \iint_{\Omega^+} \left[\bar{q}_k^+(x,\,\theta)\, u_k^+(x,\theta,h/2)(R+h/2)\right] dx\,d\theta - \iint_{\Omega^-} \left[\bar{q}_k^-(x,\,\theta)\, u_k^-(x,\theta,-h/2)(R-h/2)\right] dx\,d\theta \quad (8)$$
$$- \int_{-h/2}^{h/2} \int_{\Gamma_\sigma} \left(\bar{t}_k\, u_k\right) d\Gamma\, d\zeta - \int_{-h/2}^{h/2} \int_{\Gamma_u} \left[(u_k - \bar{u}_k)\, t_k\right] d\Gamma\, d\zeta,$$

where Ω denotes the cylinder domain on the $x-\theta$ surface, and Ω^+ and Ω^- denote the outer and inner surfaces of the cylinder (i.e., $\zeta = h/2$ and $\zeta = -h/2$), respectively, in which the transverse loads $\bar{q}_k^+$ and $\bar{q}_k^-$ $(k = x,\, \theta \text{ and } \zeta)$ are applied; Γ_σ and Γ_u denote the portions of the edge boundary, where the surface traction and displacement components (i.e., $\bar{t}_k$ and $\bar{u}_k$ (*k*= *x*, θ and ζ)) are prescribed, respectively; and $B(\sigma_{ij})$ is the complementary energy density function.

In the present formulation, we take the displacement and transverse stress components to be the primary variables subject to variation. Using the kinematic and kinetic assumptions given in Eqs. (1)–(3) and (4)–(6), respectively, we let the first-order variation of the Reissner energy functional be zero, as follows:

$$\delta\Pi_R = \sum_{m=1}^{N_l} \sum_{e=1}^{N_e} \left\{ \int_{\theta=0}^{\theta=2\pi} \int_{\bar{x}=-a/2}^{\bar{x}=a/2} \int_{\bar{\zeta}=-b/2}^{\bar{\zeta}=b/2} \left\{ \left(\delta\boldsymbol{\varepsilon}_p^{(e)}\right)^T \boldsymbol{\sigma}_p^{(e)} + \left(\delta\boldsymbol{\varepsilon}_s^{(e)}\right)^T \boldsymbol{\sigma}_s^{(e)} + \delta\varepsilon_\zeta^{(e)}\, \sigma_\zeta^{(e)} + \left(\delta\boldsymbol{\sigma}_s^{(e)}\right)^T \left(\boldsymbol{\varepsilon}_s^{(e)} - \mathbf{S}^{(m)}\boldsymbol{\sigma}_s^{(e)}\right) \right.\right.$$
$$\left.\left. + \delta\sigma_\zeta^{(e)} \left[\varepsilon_\zeta^{(e)} - \left(c_{33}^{(m)}\right)^{-1} \sigma_\zeta^{(e)} + \left(\mathbf{Q}_\zeta^{(m)}\right)^T \boldsymbol{\varepsilon}_p^{(e)}\right] \right\}^{(m)} (R+\zeta)\, d\bar{\zeta}\, d\bar{x}\, d\theta \right.$$
$$- \sum_{e=1}^{N_e} \int_{\theta=0}^{\theta=2\pi} \int_{\bar{x}=-a/2}^{\bar{x}=a/2} \left\{ \bar{q}_k^+(x,\,\theta) \left(\psi_k^{(e)}\left(\bar{x}, \bar{\zeta} = b/2\right)\right)_j^{(m=N_l)} (R+h/2) \left[\delta u_k^{(e)}\left(\bar{\zeta} = b/2\right)\right]_j^{(m=N_l)} \right\} d\bar{x}\, d\theta \quad , (9)$$
$$- \sum_{e=1}^{N_e} \int_{\theta=0}^{\theta=2\pi} \int_{\bar{x}=-a/2}^{\bar{x}=a/2} \left\{ \bar{q}_k^-(x,\,\theta) \left(\psi_k^{(e)}\left(\bar{x}, \bar{\zeta} = -b/2\right)\right)_j^{(m=1)} (R-h/2) \left[\delta u_k^{(e)}\left(\bar{\zeta} = -b/2\right)\right]_j^{(m=1)} \right\} d\bar{x}\, d\theta$$
$$= 0$$

where N_e denotes the number of cylindrical prisms in each individual layer; the superscript of *T* denotes the transposition of the matrices or vectors; and

$$\boldsymbol{\varepsilon}_p^{(e)} = \left[\varepsilon_x^{(e)} \quad \varepsilon_\theta^{(e)} \quad \gamma_{x\theta}^{(e)}\right]^T = \mathbf{B}_1^{(e)}\, \mathbf{u}^{(e)} + \mathbf{B}_2^{(e)}\, \mathbf{w}^{(e)}, \qquad \boldsymbol{\varepsilon}_s^{(e)} = \left[\gamma_{x\zeta}^{(e)} \quad \gamma_{\theta\zeta}^{(e)}\right]^T = \mathbf{B}_4^{(e)}\, \mathbf{u}^{(e)} + \mathbf{B}_5^{(e)}\, \mathbf{w}^{(e)},$$

$$\varepsilon_\zeta^{(e)} = \mathbf{B}_7^{(e)}\, \mathbf{w}^{(e)}, \qquad \boldsymbol{\sigma}_p^{(e)} = \left[\sigma_x^{(e)} \quad \sigma_\theta^{(e)} \quad \tau_{x\theta}^{(e)}\right]^T = \mathbf{Q}_p^{(m)}\, \mathbf{B}_1^{(e)}\, \mathbf{u}^{(e)} + \mathbf{Q}_p^{(m)}\, \mathbf{B}_2^{(e)}\, \mathbf{w}^{(e)} + \mathbf{Q}_\zeta^{(m)}\, \mathbf{B}_3^{(e)}\, \boldsymbol{\sigma}^{(e)},$$

$$\boldsymbol{\sigma}_s^{(e)} = \left[\tau_{x\zeta}^{(e)} \quad \tau_{\theta\zeta}^{(e)}\right]^T = \mathbf{B}_6^{(e)}\, \boldsymbol{\tau}^{(e)}, \qquad \sigma_\zeta^{(e)} = \mathbf{B}_3^{(e)}\, \boldsymbol{\sigma}^{(e)},$$

$$\mathbf{u}^{(e)} = \begin{bmatrix} u_i^{(e)} \\ v_i^{(e)} \end{bmatrix}_{i=1,2,\cdots,n_u}, \quad \mathbf{w}^{(e)} = \left[w_i^{(e)}\right]_{i=1,2,\cdots,n_w}, \quad \boldsymbol{\tau}^{(e)} = \begin{bmatrix} \left(\tau_{13}^{(e)}\right)_i \\ \left(\tau_{23}^{(e)}\right)_i \end{bmatrix}_{i=1,2,\cdots,n_\tau}, \quad \boldsymbol{\sigma}^{(e)} = \left[\left(\sigma_3^{(e)}\right)_i\right]_{i=1,2,\cdots,n_\sigma},$$

$$\mathbf{S}^{(m)}=\begin{bmatrix}\left(1/c_{55}^{(m)}\right) & 0\\ 0 & \left(1/c_{44}^{(m)}\right)\end{bmatrix},\qquad \mathbf{Q}_p^{(m)}=\begin{bmatrix}Q_{11}^{(m)} & Q_{12}^{(m)} & 0\\ Q_{12}^{(m)} & Q_{22}^{(m)} & 0\\ 0 & 0 & Q_{66}^{(m)}\end{bmatrix},\quad \mathbf{Q}_\zeta^{(m)}=\begin{bmatrix}Q_{13}^{(m)}\\ Q_{23}^{(m)}\\ 0\end{bmatrix},$$

$$\mathbf{B}_1^{(e)}=\begin{bmatrix}\left(D_x\psi_u^{(e)}\right)_i & 0\\ 0 & \left[1/(R+\zeta)\right]\left(\psi_u^{(e)}\right)_i\partial_\theta\\ \left[1/(R+\zeta)\right]\left(\psi_u^{(e)}\right)_i\partial_\theta & \left(D_x\psi_u^{(e)}\right)_i\end{bmatrix}_{i=1,2,\cdots,n_u},\qquad \mathbf{B}_2^{(e)}=\begin{bmatrix}0\\ \left[1/(R+\zeta)\right]\left(\psi_w^{(e)}\right)_i\\ 0\end{bmatrix}_{i=1,2,\cdots,n_w},$$

$$\mathbf{B}_3^{(e)}=\left[\left(\psi_\sigma^{(e)}\right)_i\right]_{i=1,2,\cdots,n_\sigma},\qquad \mathbf{B}_4^{(e)}=\begin{bmatrix}\left(D_\zeta\psi_u^{(e)}\right)_i & 0\\ 0 & \left[-1/(R+\zeta)\right]\left(\psi_u^{(e)}\right)_i+\left(D_\zeta\psi_u^{(e)}\right)_i\end{bmatrix}_{i=1,2,\cdots,n_u},$$

$$\mathbf{B}_5^{(e)}=\begin{bmatrix}\left(D_x\psi_w^{(e)}\right)_i\\ \left[1/(R+\zeta)\right]\left(\psi_w^{(e)}\right)_i\partial_\theta\end{bmatrix}_{i=1,2,\cdots,n_w},\qquad \mathbf{B}_6^{(e)}=\begin{bmatrix}\left(\psi_\tau^{(e)}\right)_i & 0\\ 0 & \left(\psi_\tau^{(e)}\right)_i\end{bmatrix}_{i=1,2,\cdots,n_\tau},\qquad \mathbf{B}_7^{(e)}=\left[\left(D_\zeta\psi_w^{(e)}\right)_i\right]_{i=1,2,\cdots,n_w},$$

$$Q_{ij}^{(m)}=c_{ij}^{(m)}-(c_{i3}^{(m)}\,c_{j3}^{(m)}/c_{33}^{(m)})\qquad (i,j=1\text{ and }2),$$

$$Q_{k3}^{(m)}=c_{k3}^{(m)}/c_{33}^{(m)}\qquad (k=1\text{ and }2),\qquad Q_{66}^{(m)}=c_{66}^{(m)}.$$

2.3. Euler–Lagrange equations

The static behavior of a multilayered FGM/FRCM cylinder with various boundary edges and under mechanical loads is studied in the following illustrative examples, in which the two edges are considered as combinations of clamped and simply supported edges. The applied loading conditions on the lateral surfaces of the cylinder are prescribed as

$$\left[\tau_{x\zeta}^{(N_l)}(x,\theta,h/2)\quad \tau_{\theta\zeta}^{(N_l)}(x,\theta,h/2)\quad \sigma_\zeta^{(N_l)}(x,\theta,h/2)\right]=\left[0\quad 0\quad \bar{q}_\zeta^{+}(x,\theta)\right]\qquad \text{on}\quad \zeta=h/2,\quad (10a)$$

$$\left[\tau_{x\zeta}^{(1)}(x,\theta,-h/2)\quad \tau_{\theta\zeta}^{(1)}(x,\theta,-h/2)\quad \sigma_\zeta^{(1)}(x,\theta,-h/2)\right]=\left[0\quad 0\quad \bar{q}_\zeta^{-}(x,\theta)\right]\qquad \text{on}\quad \zeta=-h/2,\quad (10b)$$

where $\bar{q}_\zeta^{\pm}$ are expressed as the single Fourier series and given as $\bar{q}_\zeta^{\pm}=\sum_{\hat{n}=0}^{\infty}q_{\hat{n}}^{\pm}\cos(\hat{n}\,\theta)$ in which $\hat{n}$ is a positive integer or zero.

As mentioned above, the boundary edges at $x=0$ and $x=L$ are a combination of clamped and simply supported edges, the corresponding boundary conditions of which are given as follows:

For clamped (C) supports,

$$u_x^{(e)}=u_\theta^{(e)}=u_\zeta^{(e)}=0.\qquad (11a)$$

For simple (S) supports,

$$u_{\theta}^{(e)} = u_{\zeta}^{(e)} = \sigma_{x}^{(e)} = 0 . \tag{11b}$$

By means of the separation of variables, the primary field variables of each individual cylindrical layer in Eqs. (1)–(6) are expanded as the single Fourier series in the circumferential coordinate, and they are rewritten as

$$\left(u_{x}^{(e)}\right)^{(m)} = \sum_{\hat{n}=0}^{\infty}\sum_{i=1}^{n_u}\left(\psi_{u}^{(e)}\right)_i\left(u_{\hat{n}}^{(e)}\right)_i^{(m)}\cos\hat{n}\theta \ , \tag{12}$$

$$\left(u_{\theta}^{(e)}\right)^{(m)} = \sum_{\hat{n}=0}^{\infty}\sum_{i=1}^{n_u}\left(\psi_{u}^{(e)}\right)_i\left(v_{\hat{n}}^{(e)}\right)_i^{(m)}\sin\hat{n}\theta \ , \tag{13}$$

$$\left(u_{\zeta}^{(e)}\right)^{(m)} = \sum_{\hat{n}=0}^{\infty}\sum_{j=1}^{n_w}\left(\psi_{w}^{(e)}\right)_j\left(w_{\hat{n}}^{(e)}\right)_j^{(m)}\cos\hat{n}\theta , \tag{14}$$

$$\left(\tau_{x\zeta}^{(e)}\right)^{(m)} = \sum_{\hat{n}=0}^{\infty}\sum_{k=1}^{n_\tau}\left(\psi_{\tau}^{(e)}\right)_k\left(\tau_{13\hat{n}}^{(e)}\right)_k^{(m)}\cos\hat{n}\theta \ , \tag{15}$$

$$\left(\tau_{\theta\zeta}^{(e)}\right)^{(m)} = \sum_{\hat{n}=0}^{\infty}\sum_{k=1}^{n_\tau}\left(\psi_{\tau}^{(e)}\right)_k\left(\tau_{23\hat{n}}^{(e)}\right)_k^{(m)}\sin\hat{n}\theta \ , \tag{16}$$

$$\left(\sigma_{\zeta}^{(e)}\right)^{(m)} = \sum_{\hat{n}=0}^{\infty}\sum_{l=1}^{n_\sigma}\left(\psi_{\sigma}^{(e)}\right)_l\left(\sigma_{3\hat{n}}^{(e)}\right)_l^{(m)}\cos\hat{n}\theta \ . \tag{17}$$

Introducing the kinetic and kinematic models of the FCPMs (Eqs. (12)–(17)) and the boundary coditions on the lateral surfaces (Eqs. (10a) and (10b)) in Eq. (9), then imposing the stationary principle of the Reissner energy functional (i.e., $\delta\Pi_R = 0$), we thus obtain the Euler–Lagrange equations of the cylinder as follows:

$$\sum_{m=1}^{N_l}\sum_{e=1}^{N_e}\begin{bmatrix} \mathbf{K}_{\mathbf{I}\ \mathbf{I}}^{(e)} & \mathbf{K}_{\mathbf{I}\ \mathbf{II}}^{(e)} & \mathbf{K}_{\mathbf{I}\ \mathbf{III}}^{(e)} & \mathbf{K}_{\mathbf{I}\ \mathbf{IV}}^{(e)} \\ \mathbf{K}_{\mathbf{II}\ \mathbf{I}}^{(e)} & \mathbf{K}_{\mathbf{II}\ \mathbf{II}}^{(e)} & \mathbf{K}_{\mathbf{II}\ \mathbf{III}}^{(e)} & \mathbf{K}_{\mathbf{II}\ \mathbf{IV}}^{(e)} \\ \mathbf{K}_{\mathbf{III}\ \mathbf{I}}^{(e)} & \mathbf{K}_{\mathbf{III}\ \mathbf{II}}^{(e)} & \mathbf{K}_{\mathbf{III}\ \mathbf{III}}^{(e)} & \mathbf{0} \\ \mathbf{K}_{\mathbf{IV}\ \mathbf{I}}^{(e)} & \mathbf{K}_{\mathbf{IV}\ \mathbf{II}}^{(e)} & \mathbf{0} & \mathbf{K}_{\mathbf{IV}\ \mathbf{IV}}^{(e)} \end{bmatrix}^{(m)}\begin{bmatrix} \widetilde{\mathbf{u}}^{(e)} \\ \widetilde{\mathbf{w}}^{(e)} \\ \widetilde{\boldsymbol{\tau}}^{(e)} \\ \widetilde{\boldsymbol{\sigma}}^{(e)} \end{bmatrix}^{(m)} = \delta_{m1}\sum_{e=1}^{N_e}\begin{bmatrix} \mathbf{0} \\ \mathbf{Q}_1^{(e)} \\ \mathbf{0} \\ \mathbf{0} \end{bmatrix}^{(m)} + \delta_{mN_l}\sum_{e=1}^{N_e}\begin{bmatrix} \mathbf{0} \\ \mathbf{Q}_{N_l}^{(e)} \\ \mathbf{0} \\ \mathbf{0} \end{bmatrix}^{(m)} , \tag{18}$$

where $\left(\mathbf{K}_{i\ j}^{(e)}\right)^{(m)} = \left[\left(\mathbf{K}_{j\ i}^{(e)}\right)^{(m)}\right]^T$ $(i, j = \mathbf{I},\ \mathbf{II},\ \mathbf{III},\ \mathbf{IV})$; $\left(\mathbf{K}_{\mathbf{I}\ \mathbf{I}}^{(e)}\right)^{(m)} = \int_{-b/2}^{b/2}\int_{-a/2}^{a/2}\left(\widetilde{\mathbf{B}}_1^{(e)}\right)^T\mathbf{Q}_p^{(m)}\widetilde{\mathbf{B}}_1^{(e)}\left(R+\zeta\right)d\bar{x}\,d\bar{\zeta}$,

$\left(\mathbf{K}_{\mathbf{I}\ \mathbf{II}}^{(e)}\right)^{(m)} = \int_{-b/2}^{b/2}\int_{-a/2}^{a/2}\left(\widetilde{\mathbf{B}}_1^{(e)}\right)^T\mathbf{Q}_p^{(m)}\mathbf{B}_2^{(e)}\left(R+\zeta\right)d\bar{x}\,d\bar{\zeta}$, $\left(\mathbf{K}_{\mathbf{I}\ \mathbf{III}}^{(e)}\right)^{(m)} = \int_{-b/2}^{b/2}\int_{-a/2}^{a/2}\left(\mathbf{B}_4^{(e)}\right)^T\mathbf{B}_6^{(e)}\left(R+\zeta\right)d\bar{x}\,d\bar{\zeta}$,

$\left(\mathbf{K}_{\mathbf{I}\ \mathbf{IV}}^{(e)}\right)^{(m)} = \int_{-b/2}^{b/2}\int_{-a/2}^{a/2}\left(\widetilde{\mathbf{B}}_1^{(e)}\right)^T\mathbf{Q}_\zeta^{(m)}\mathbf{B}_3^{(e)}\left(R+\zeta\right)d\bar{x}\,d\bar{\zeta}$, $\left(\mathbf{K}_{\mathbf{II}\ \mathbf{II}}^{(e)}\right)^{(m)} = \int_{-b/2}^{b/2}\int_{-a/2}^{a/2}\left(\mathbf{B}_2^{(e)}\right)^T\mathbf{Q}_p^{(m)}\mathbf{B}_2^{(e)}\left(R+\zeta\right)d\bar{x}\,d\bar{\zeta}$,

$$\left(\mathbf{K}_{\mathbf{II}\ \mathbf{III}}^{(e)}\right)^{(m)}=\int_{-b/2}^{b/2}\int_{-a/2}^{a/2}\left(\widetilde{\mathbf{B}}_5^{(e)}\right)^T\mathbf{B}_6^{(e)}\left(R+\zeta\right)d\bar{x}\,d\bar{\zeta}\ ,\qquad \left(\mathbf{K}_{\mathbf{II}\ \mathbf{IV}}^{(e)}\right)^{(m)}=\int_{-b/2}^{b/2}\int_{-a/2}^{a/2}\left[\left(\mathbf{B}_2^{(e)}\right)^T\mathbf{Q}_\zeta^{(m)}\mathbf{B}_3^{(e)}+\left(\mathbf{B}_7^{(e)}\right)^T\mathbf{B}_3^{(e)}\right]\left(R+\zeta\right)d\bar{x}\,d\bar{\zeta}\ ,$$

$$\left(\mathbf{K}_{\mathbf{III}\ \mathbf{III}}^{(e)}\right)^{(m)}=-\int_{-b/2}^{b/2}\int_{-a/2}^{a/2}\left(\mathbf{B}_6^{(e)}\right)^T\mathbf{S}^{(m)}\mathbf{B}_6^{(e)}\left(R+\zeta\right)d\bar{x}\,d\bar{\zeta}\ ,\qquad \left(\mathbf{K}_{\mathbf{IV}\ \mathbf{IV}}^{(e)}\right)^{(m)}=-\int_{-b/2}^{b/2}\int_{-a/2}^{a/2}\left(1/c_{33}^{(m)}\right)\left(\mathbf{B}_3^{(e)}\right)^T\mathbf{B}_3^{(e)}\left(R+\zeta\right)d\bar{x}\,d\bar{\zeta}\ ,$$

$$\widetilde{\mathbf{B}}_1^{(e)}=\begin{bmatrix}\left(D_x\psi_u^{(e)}\right)_i & 0\\ 0 & \hat{n}\left[1/\left(R+\zeta\right)\right]\left(\psi_u^{(e)}\right)_i\\ -\hat{n}\left[1/\left(R+\zeta\right)\right]\left(\psi_u^{(e)}\right)_i & \left(D_x\psi_u^{(e)}\right)_i\end{bmatrix}_{i=1,2,\cdots,n_u},\qquad \widetilde{\mathbf{B}}_5^{(e)}=\begin{bmatrix}\left(D_x\psi_w^{(e)}\right)_i\\ -\hat{n}\left[1/\left(R+\zeta\right)\right]\left(\psi_w^{(e)}\right)_i\end{bmatrix}_{i=1,2,\cdots,n_w},$$

$$\widetilde{\mathbf{u}}^{(m)}=\begin{bmatrix}\left(u_{\hat{n}}^{(e)}\right)_i^{(m)}\\ \left(v_{\hat{n}}^{(e)}\right)_i^{(m)}\end{bmatrix}_{i=1,2,\cdots,n_u},\qquad \widetilde{\mathbf{w}}^{(m)}=\left[\left(w_{\hat{n}}^{(e)}\right)_i^{(m)}\right]_{i=1,2,\cdots,n_w},\qquad \widetilde{\boldsymbol{\tau}}^{(m)}=\begin{bmatrix}\left(\tau_{13\hat{n}}^{(e)}\right)_i^{(m)}\\ \left(\tau_{23\hat{n}}^{(e)}\right)_i^{(m)}\end{bmatrix}_{i=1,2,\cdots,n_\tau},$$

$$\widetilde{\boldsymbol{\sigma}}^{(m)}=\left[\left(\sigma_{3\hat{n}}^{(e)}\right)_i^{(m)}\right]_{i=1,2,\cdots,n_\sigma},\qquad \left(\mathbf{Q}_1^{(e)}\right)^{(m=N_l)}=\int_{-a/2}^{a/2}\left(q_{\hat{n}}^-\right)\mathbf{B}_8^{(e)}\left(R-h/2\right)d\bar{x}\ ,\quad \left(\mathbf{Q}_{N_l}^{(e)}\right)^{(m=N_l)}=\int_{-a/2}^{a/2}\left(q_{\hat{n}}^+\right)\mathbf{B}_9^{(e)}\left(R+h/2\right)d\bar{x}\ ,$$

$$\mathbf{B}_8^{(e)}=\left[\left(\psi_w^{(e)}\left(\bar{x},\bar{\zeta}=-b/2\right)\right)_i\right]_{i=1,2,\cdots,n_w},\quad \mathbf{B}_9^{(e)}=\left[\left(\psi_w^{(e)}\left(\bar{x},\bar{\zeta}=b/2\right)\right)_i\right]_{i=1,2,\cdots,n_w};$$

and the symbols of $\delta_{m\,1}\ \ (m=1,2,\cdots,N_l)$ and $\delta_{m\,N_l}\ \ (m=1,2,\cdots,N_l)$ are the Kronecker delta functions, in which $\delta_{m\,j}=0$ when $m\neq j$, and $\delta_{j\,j}=1$.

Using Eq. (18) and assembling both the local stiffness matrix and forcing vector of each prism constituting the cylinder by following the standard process of the FEMs, in which the displacement and transverse stress continuity conditions at the interfaces between adjacent prisms are imposed and thus satisfied a priori for the unified formulation of these RMVT-based FCPMs, we can construct the corresponding global stiffness matrix and forcing vector for the cylinder. The primary variables at each node of the prism can then be determined. Subsequently, the variables of the in-surface stresses at the nodes can be obtained using the determined primary variables, and these are given by

$$\left(\sigma_x^{(e)},\ \sigma_\theta^{(e)}\right)^{(m)}=\sum_{\hat{n}=0}^{\infty}\left(\sigma_{1\hat{n}}^{(e)},\ \ \sigma_{2\hat{n}}^{(e)}\right)^{(m)}\cos\hat{n}\,\theta\ , \tag{19}$$

$$\left(\tau_{x\theta}^{(e)}\right)^{(m)}=\sum_{n=0}^{\infty}\left(\tau_{12\hat{n}}^{(e)}\right)^{(m)}\ \sin\hat{n}\,\theta\ , \tag{20}$$

where $\left[\left(\sigma_{1\hat{n}}^{(e)}\right)^{(m)}\quad\left(\sigma_{2\hat{n}}^{(e)}\right)^{(m)}\quad\left(\tau_{12\hat{n}}^{(e)}\right)^{(m)}\right]^T=\mathbf{Q}_p^{(m)}\widetilde{\mathbf{B}}_1^{(e)}\widetilde{\mathbf{u}}^{(e)}+\mathbf{Q}_p^{(m)}\mathbf{B}_2^{(e)}\widetilde{\mathbf{w}}^{(e)}+\mathbf{Q}_\zeta^{(m)}\mathbf{B}_3^{(e)}\widetilde{\boldsymbol{\sigma}}^{(e)}$.

Using the unified formulation of RMVT-based FCPMs, we investigate the 3D static behaviors of LC cylinders with various boundary conditions and under mechanical loads in the following illustrative examples, and the performances of the RMVT-based L4, Q8 and Q9 FCPMs are also examined.

3. ILLUSTRATIVE EXAMPLES

3.1 Laminated orthotropic cylinders

A benchmark problem for the 3D bending analysis of simply supported, laminated orthotropic circular hollow cylinders subject to a sinusoidally distributed load ($\bar{q}_{\zeta}^{+}=0$ and $\bar{q}_{\zeta}^{-}=q_0\sin(\pi x/L)\cos 4\theta$) was presented by Varadan and Bhaskar (1991), and these exact 3D solutions are used to validate the accuracy and convergence of the present RMVT-based FCPMs. The material properties of the cylinders are given as

$$E_L=25\text{x}10^6 \text{ psi } (172.4 \text{ GPa}), \qquad E_T=1.0\text{x}10^6 \text{ psi } (6.89 \text{ GPa}),$$

$$G_{LT}=0.5\text{x}10^6 \text{ psi } (3.45 \text{ GPa}), \qquad G_{TT}=0.2\text{x}10^6 \text{ psi } (1.378 \text{ GPa}),$$

$$\upsilon_{LL}=\upsilon_{LT}=0.25, \tag{21a-e}$$

where the subscripts of *L* and *T* denote the directions parallel and transverse to the fiber directions, respectively.

For comparison purposes, the set of normalized variables used in Varadan and Bhaskar (1991) is defined as

$$[\bar{u}_x(\zeta),\ \bar{u}_\theta(\zeta)]=\frac{10\,E_L}{q_0\,h\,S^3}\left[u_x(0,0,\zeta),\ u_\theta\left(\frac{L}{2},\frac{\pi}{8},\zeta\right)\right], \qquad \bar{u}_r(\zeta)=\frac{10\,E_L}{q_0\,h\,S^4}u_r\left(\frac{L}{2},\ 0,\ \zeta\right),$$

$$[\bar{\sigma}_x(\zeta),\ \bar{\sigma}_\theta(\zeta),\ \bar{\tau}_{x\theta}(\zeta)]=\frac{10}{q_0\,S^2}\left[\sigma_x\left(\frac{L}{2},\ 0,\ \zeta\right),\ \sigma_\theta\left(\frac{L}{2},\ 0,\ \zeta\right),\ \tau_{x\theta}\left(0,\ \frac{\pi}{8},\ \zeta\right)\right],$$

$$[\bar{\tau}_{xr}(\zeta),\ \bar{\tau}_{\theta r}(\zeta)]=\frac{10}{q_0\,S}\left[\tau_{xr}(0,\ 0,\ \zeta),\ \tau_{\theta r}\left(\frac{L}{2},\ \frac{\pi}{8},\ \zeta\right)\right], \qquad \bar{\sigma}_r(\zeta)=\sigma_r\left(\frac{L}{2},0,\ \zeta\right)/q_0, \tag{22a-e}$$

in which *S*=*R*/*h*.

Table 1 shows the convergence studies for the L4, Q8 and Q9 FCPM solutions of displacement and stress components induced at the crucial positions of simply supported, $[90^0/0^0/90^0]$ laminated hollow cylinders, in which $L/R=4$, and R/h=4 and 10, and the meshes used in $x-\zeta$ surface are (36x6), (48x9) and (60x12) for the L4 FCPM, as well as (36x6), (48x9) and (48x12) for the Q8 and Q9 ones. It can be seen in Table 1 that for a moderately thick cylinder (*R*/*h*=10) the convergent solutions of the Q8 and Q9 FCPMs are obtained with the (48x12) mesh and those of the L4 FCPM with the (60x12) one, and that the convergence speed decreases when the cylinder becomes thicker, while the Q8/Q9 solutions with the (48x12) mesh are in excellent agreement with the exact 3D ones obtained using Pagano and modified Pagano methods by Varadan and Bhaskar (1991) and Wu and Tsai (2012), respectively, as well as the 9-layer quadratic PVD- and RMVT-based FCLM solutions (i.e., LD_{22} and LM_{22}^{22} with $N_l=9$) by Wu and Kuo (2013) and Wu and Chang (2012).

Table 1
Convergence studies for the RMVT-based FCPM solutions of the displacement and stress components at the crucial positions of $[90^0/0^0/90^0]$ laminated cylinders with fully simple supports and under the sinusoidally distributed load (L/R=4).

(R/h)	Theories	$\bar{\sigma}_x(h/2)$	$\bar{\sigma}_\theta(h/2)$	$\bar{\tau}_{x\theta}(h/2)$	$\bar{\sigma}_r(-h/6)$	$\bar{\tau}_{\theta r}(-h/6)$	$\bar{u}_r(0)$
4	Present L4 (36x6)	0.11427	6.41770	0.10713	-0.85597	-2.87581	3.98391
	Present L4 (48x9)	0.12459	6.50901	0.10780	-0.79312	-2.50876	4.00110
	Present L4 (60x12)	0.12351	6.53179	0.10802	-0.82832	-2.62670	4.00526
	Present Q8 (36x6)	0.12384	6.53353	0.10798	-0.83068	-2.63859	4.00560
	Present Q8 (48x9)	0.12559	6.54145	0.10805	-0.82212	-2.57613	4.00879
	Present Q8 (48x12)	0.12623	6.54325	0.10806	-0.81889	-2.55330	4.00856
	Present Q9 (36x6)	0.12383	6.53334	0.10798	-0.83070	-2.63869	4.00559
	Present Q9 (48x9)	0.12559	6.54140	0.10805	-0.82211	-2.57612	4.00879
	Present Q9 (48x12)	0.12623	6.54323	0.10806	-0.81889	-2.55332	4.00856
	LD_{11} (N_l=9)	0.1117	6.3458	0.1065	-0.8097	-2.5006	3.9662
	LD_{22} (N_l=9)	0.1266	6.5411	0.1081	-0.8144	-2.5224	4.0080
	LM_{11}^{11} (N_l=9)	0.1246	6.5067	0.1077	-0.7928	-2.5079	3.9997
	LM_{22}^{22} (N_l=9)	0.1256	6.5412	0.1081	-0.8221	-2.5761	4.0087
	3D elasticity	0.1270	6.545	0.1081	NA	NA	4.009
	Modified Pagano	0.12703	6.54455	0.10808	-0.81460	-2.52326	4.00895
10	Present L4 (36x6)	0.07162	4.67828	0.03741	-1.58544	-3.55657	1.22335
	Present L4 (48x9)	0.07401	4.68273	0.03741	-1.48214	-3.34495	1.22340
	Present L4 (60x12)	0.07334	4.68276	0.03741	-1.53030	-3.40162	1.22346
	Present Q8 (36x6)	0.07337	4.68199	0.03737	-1.53130	-3.40312	1.22323
	Present Q8 (48x9)	0.07368	4.68250	0.03738	-1.52001	-3.37252	1.22330
	Present Q8 (48x12)	0.07379	4.68268	0.03738	-1.51597	-3.36168	1.22329
	Present Q9 (36x6)	0.07337	4.68198	0.03737	-1.53134	-3.40319	1.22323
	Present Q9 (48x9)	0.07368	4.68250	0.03738	-1.51999	-3.37250	1.22330
	Present Q9 (48x12)	0.07379	4.68268	0.03738	-1.51598	-3.36169	1.22329
	LD_{11} (N_l=9)	0.0704	4.6492	0.0372	-1.5103	-3.3464	1.2188
	LD_{22} (N_l=9)	0.0738	4.6824	0.0374	-1.5108	-3.3476	1.2233
	LM_{11}^{11} (N_l=9)	0.0740	4.6811	0.0374	-1.4816	-3.3438	1.2230
	LM_{22}^{22} (N_l=9)	0.0737	4.6823	0.0374	-1.5200	-3.3724	1.2233
	3D elasticity	0.0739	4.683	0.0374	NA	NA	1.223
	Modified Pagano	0.07392	4.68272	0.03739	-1.51082	-3.34769	1.22329

Table 2 shows the present Q9 FCPM solutions of displacement and stress components induced at the crucial positions of the $[0^0/90^0/0^0]$ laminated cylinders with SS, CC and SC edge conditions and under a uniformly distributed load (i.e., $\bar{q}_\zeta^+ = 0$ and $\bar{q}_\zeta^- = q_0$), in which L/R=5 and R/h=5, and the meshes used in $x-\zeta$ surface are (36x6), (48x9) and (48x12). It can be seen that the convergent solutions of Q9 FCPMs are obtained when the (48x12) mesh is used, and these closely agree with the accurate solutions obtained using the state space-based DRK method (Wu and Jiang, 2012) and the ANSYS software, in which the number of sampling nodes is taken to be 41 in the

former method, and a 20-node brick element with the (40x13x9), (80x26x9) and (120x39x9) meshes in the (x, θ, ζ) directions is used in the ANSYS software. In this example, the deflections at the center of the cylinders with various boundary conditions are SS>SC>CC.

Table 2
Convergence studies for the RMVT-based FCPM solutions of the displacement and stress components of $[0^0/90^0/0^0]$ laminated cylinders with various boundary conditions and under a uniformly distributed load (*L*/*R*=5, *R*/*h*=5).

Variables	Theories	SS	CC	SC
$\bar{u}_r(0)$	Q9 FCPM (36x6)	1.01840	1.01758	1.01797
	Q9 FCPM (48x9)	1.01839	1.01764	1.01800
	Q9 FCPM (48x12)	1.01840	1.01752	1.01794
	State space DRKM	1.0192	1.0177	1.0185
	ANSYS (1/4 model, 40 x 13 x 9)	1.0190	1.0176	1.0183
	ANSYS (1/4 model, 80 x 26 x 9)	1.0190	1.0176	1.0183
	ANSYS (1/4 model, 120 x 39 x 9)	1.0190	1.0176	1.0183
$\bar{\sigma}_x(0)$	Q9 FCPM (36x6)	0.00663	0.00643	0.00663
	Q9 FCPM (48x9)	0.00640	0.00620	0.00640
	Q9 FCPM (48x12)	0.00649	0.00628	0.00649
	State space DRKM	0.00644	0.00620	0.00643
	ANSYS (1/4 model, 40 x 13 x 9)	0.00636	0.00616	0.00636
	ANSYS (1/4 model, 80 x 26 x 9)	0.00640	0.00617	0.00639
	ANSYS (1/4 model, 120 x 39 x 9)	0.00643	0.00619	0.00641
$\bar{\sigma}_r(0)$	Q9 FCPM (36x6)	-0.43822	-0.43819	-0.43820
	Q9 FCPM (48x9)	-0.44053	-0.44049	-0.44051
	Q9 FCPM (48x12)	-0.43963	-0.43960	-0.43962
	State space DRKM	-0.4401	-0.4401	-0.4401
	ANSYS (1/4 model, 40 x 13 x 9)	-0.4337	-0.4337	-0.4337
	ANSYS (1/4 model, 80 x 26 x 9)	-0.4390	-0.4389	-0.4389
	ANSYS (1/4 model, 120 x 39 x 9)	-0.4399	-0.4399	-0.4399

4. CONCLUDING REMARKS

In this work, we have developed a unified formulation of various RMVT-based FCPMs to investigate the static behaviors of multilayered composite cylinders, and homogeneous and FGM sandwich ones with combinations of the simply-supported and clamped edges and under mechanical loads. Implementing these FCPMs shows the Q8 and Q9 FCPM solutions closely agree with each other, and their convergent solutions are in excellent agreement with the exact 3D ones for simply-supported, laminated composite cylinders and FGM sandwich ones available in the literature.

ACKNOWLEDGMENTS
This work was supported by the National Science Council of Republic of China through grant NSC 100-2221-E-006-180-MY3.

REFERENCES

Akhras, G. and Li, W.C. (2007), "Three-dimensional static, vibration and stability analysis of piezoelectric composite plates using a finite layer method," *Smart Mater. Struct.* **16**, 561-569.

Akhras, G. and Li, W.C. (2008), "Three-dimensional thermal buckling analysis of piezoelectric composite plates using the finite layer method," *Smart Mater. Struct*., **17**, 1-8.

Akhras, G. and Li, W.C. (2010), "Three-dimensional stability analysis of piezoelectric antisymmetric angle-ply laminates using finite layer method," *J. Intell. Mater. Sys. Struct*., **21**, 719-727.

Carrera, E. (2000a), "An assessment of mixed and classical theories on global and local response of multilayered orthotropic plates," *Compos. Struct.*, **50**, 183-198.

Carrera, E. (2000b), "A priori vs. a posteriori evaluation of transverse stresses in multilayered orthotropic plates," *Compos. Struct.*, **48**, 245-260.

Carrera, E. (2000c), "An assessment of mixed and classical theories on global and local response of multilayered orthotropic plates," *Compos. Struct*., **50**, 183-198.

Carrera, E. (2001), "Developments, ideas, and evaluations based upon Reissner's Mixed Variational Theorem in the modeling of multilayered plates and shells," *Appl. Mech. Rev*., **54**, 301-329.

Carrera, E. (2003), "Historical review of zig-zag theories for multilayered plates and shells," *Appl. Mech. Rev.*, **56**, 287-308.

Carrera, E. and Ciuffreda, A. (2005), "A unified formulation to assess theories of multilayered plates for various bending problems," *Compos. Struct*. **69**, 271-293.

Carrera, E. and Petrolo, M. (2010), "Guidelines and recommendations to construct theories for metallic and composite plates," *AIAA. J.*, **48**, 2852-2866.

Carrera, E., Brischetto, S., Cinefra, M. and Soave, M. (2010), "Refined and advanced models for multilayered plates and shells embedding functionally graded material layers," *Mech. Adv. Mater. Struct*., **17**, 603-621.

Cheung, Y.K. and Jiang, C.P. (2001), "Finite layer method in analysis of piezoelectric composite laminates," *Comput. Methods Appl. Mech. Engrg*., **191**, 879–901.

Noor, A.K. and Burton, W.S. (1990a), "Assessment of computational models for multilayered anisotropic plates," *Compos. Struct*., **14**, 233-265.

Noor, A.K. and Burton, W.S. (1990b), "Assessment of computational models for multilayered composite shells," *Appl. Mech. Rev*., **43**, 67-97.

Noor, A.K., Burton, W.S. and Peters, J.M. (1991), "Assessment of computational models for multilayered composite cylinders," *Int. J. Solids Struct*., **27**, 1269-1286.

Noor, A.K., Burton, W.S. and Bert, C.W. (1996), "Computational model for sandwich panels and shells," *Appl. Mech. Rev*., **49**, 155-199.

Varadan, T.K. and Bhaskar, K. (1991), "Bending of laminated orthotropic cylindrical shells-An elasticity approach," *Compos. Struct*., **17**, 141-156.

Wu, C.P. and Chang, Y.T. (2012), "A unified formulation of RMVT-based finite cylindrical layer methods for sandwich circular hollow cylinders with an embedded FGM layer," *Compos. Part B Eng*., **43**, 3318-3333.

Wu, C.P. and Jiang, R.Y. (2010), “A state space differential reproducing kernel method for the analysis of FGM sandwich circular hollow cylinders with combinations of simply-supported and clamped edges,” *Compos. Struct*., **94**, 3401-3420.
Wu, C.P. and Kuo, C.H. (2013), “A unified formulation of PVD-based finite cylindrical layer methods for functionally graded material sandwich cylinders,” *Appl. Math. Model.*, **37**, 916-938.
Wu, C.P. and Li, H.Y. (2010), “The RMVT- and PVD-based finite layer methods for the three-dimensional analysis of multilayered composite and FGM plates,” *Compos. Struct.*, **92**, 2476-2496.
Wu, C.P. and Tsai, T.C. (2012), “Exact solutions of functionally graded piezoelectric material sandwich cylinders by a modified Pagano method,” *Appl. Math. Model*., **36**, 1910-1930.
Wu, C.P., Chiu, K.H. and Wang, Y.M. (2008), “A review on the three-dimensional analytical approaches of multilayered and functionally graded piezoelectric plates and shells,” *CMC-Comput. Mater. Continua*, **8**, 93-133.